The Scattering of a Continental Shelf Wave by a Long Thin Barrier Lying Parallel to the Coast

WILLIAM W. HSIEH[1] AND V. T. BUCHWALD

School of Mathematics, University of New South Wales, Kensington, N.S.W., Australia 2033

(Manuscript received 9 September 1984, in final form 22 January 1985)

ABSTRACT

The scattering of an incident shelf wave by a long thin offshore barrier located parallel to the coast is solved for a general monotonically increasing depth profile, using the unforced, inviscid barotropic shallow water equations under rigid lid and alongshore geostrophy approximations. In particular, simple analytic formulas for the scattering coefficients are derived for the exponential shelf profile. In the channel between the barrier and the coast, much of the incident shelf wave energy is transferred to the zero (or Kelvin) mode. Seaward of the barrier, substantial energy transfer from an incident second-mode shelf wave to the first mode is possible. Downstream from the barrier, the incident mode may vanish, leaving a different mode to dominate.

1. Introduction

Low-frequency coastally-trapped waves are now known to propagate along the continental shelf in many parts of the world. The continental shelf is in reality punctuated by topographic irregularities—in particular, a long thin island or a chain of islands is often found lying offshore, parallel to the coastline. Along the North American coast, examples include Long Island, Vancouver Island, Queen Charlotte Islands, and the Baja California peninsula. Elsewhere, we find Taiwan off China, Madagascar off Africa, the Hebrides off Scotland, and the Great Barrier Reef off northeast Australia. Hence, we investigate the consequences of a continental shelf wave encountering a long thin offshore barrier lying parallel to the coast. Even for islands which are not of a long thin shape, e.g. Tasmania, our theory qualitatively predicts some interesting phenomena.

Theoretical papers on the scattering of shelf waves by topography include Allen (1976) and Grimshaw (1977), where topography varies slowly alongshore; Buchwald (1977) and Chao *et al.* (1979), where a small bump is located at the coastline and on the shelf, respectively; Brink (1980), where the shelf has small random bottom irregularities; Wang (1980), where the effects of submarine canyons and ridges are studied numerically; Davis (1981), where a headland protrudes into the shelf; and Hsieh and Buchwald (1984, henceforth referred to as HB).

In HB, a first-mode shelf wave propagating along a step-shaped shelf is scattered by a semi-infinitely long barrier (of negligible width) placed along the outer edge of the flat shelf. Using a Wiener-Hopf technique, HB found that within the flat channel enclosed by the barrier, the incoming energy flux from the first-mode shelf wave is essentially all transferred to the zero channel mode, which corresponds to the Kelvin wave modified by the rigid-lid approximation.

The major disadvantage of the HB theory, that of using a step shelf (where only the first-mode shelf wave can propagate freely) has been overcome in this study, where the bottom topography h as a function of the offshore distance y is only required to be monotonically increasing ($dh/dy > 0$) with dh/dy piecewise continuous. This yields a Sturm-Liouville problem with complete orthonormal eigenfunctions. The scattering problem is solved by simple eigenfunction matching rather than by the more complicated Wiener-Hopf technique in HB. Furthermore, in contrast to HB, the barrier can now be of finite length, and may be placed any distance offshore (Fig. 1).

The basic theory and the general solution for any monotonically increasing topography $h(y)$ are developed in Sections 2 and 3. In Section 4, specializing to the exponential shelf profile where h increases exponentially with y, we derive simple analytic formulas for the scattering coefficients. The limitations of our theory are discussed in Section 5.

2. Basic theory

Assume a straight coastline at $y = 0$, and a monotonically increasing depth $h = h(y)$ for $y > 0$, [with $h(0) > 0$] (Fig. 1). We nondimensionalize the horizontal spatial variables x and y with respect to the shelf/slope width, and time t, with respect to f^{-1} (f being the constant Coriolis parameter), so that the

[1] Current affiliation: Dept. of Oceanography, University of British Columbia, Vancouver, B.C. Canada V6T 1W5.

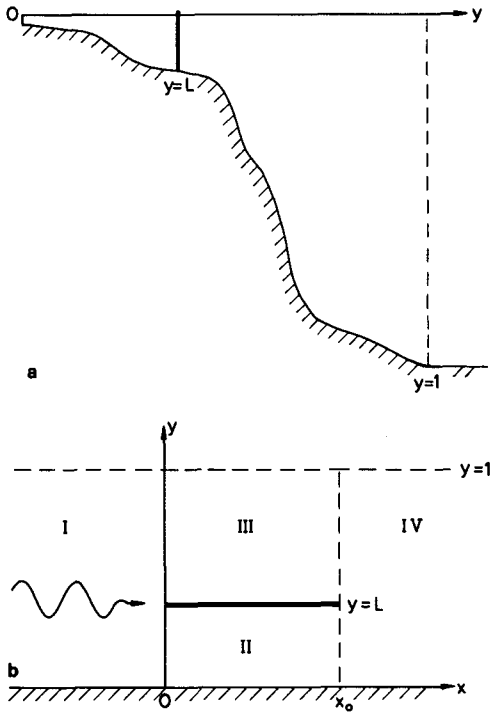

FIG. 1. The geometry of the problem, (a) side view and (b) plan view. The continental shelf is described by a monotonically increasing depth $h(y)$, with nonzero depth at the coast. A long, infinitely thin but impermeable barrier is located at $y = L$, $0 < x < x_0$. An approximate outer boundary condition $u = 0$ is imposed at $y = 1$. Four regions I, II, III and IV are marked in (b), with the incident shelf wave approaching from region I.

unforced barotropic shallow water equations in a rotating, frictionless fluid can be written as

$$u_t - v = -p_x, \tag{2.1a}$$

$$u = -p_y, \tag{2.1b}$$

$$(hu)_x + (hv)_y = 0, \tag{2.1c}$$

where the alongshore geostrophy approximation and the rigid-lid approximation have been used in (2.1b) and (2.1c) respectively. Cross-differentiate (2.1a and b) to eliminate p, then substitute in the transport stream function ψ,

$$\psi = \Phi(y)e^{i(kx-\omega t)}, \quad hu = \psi_y, \quad hv = -\psi_x, \tag{2.2}$$

to get an ordinary differential equation for Φ,

$$\left(\frac{1}{h}\Phi'\right)' + \frac{1}{c}\frac{h'}{h^2}\Phi = 0, \tag{2.3}$$

where prime denotes d/dy and $c = \omega/k$.

For boundary conditions, we require no normal flow through the small coastal wall and through the barrier, i.e. $v = 0$ at $y = 0$, and at $y = L$, $0 < x < x_0$. By the third equation in (2.2), ψ must remain (spatially) constant along $y = 0$ and $y = L$, $0 < x < x_0$. Without loss of generality, we choose the constants so that

$$\psi = 0 \quad \text{at} \quad y = 0, \tag{2.4}$$

$$\psi = B_0 e^{-i\omega t} \quad \text{at} \quad y = L, \quad 0 < x < x_0. \tag{2.5}$$

It is clear from (2.2) that (2.5) can only be satisfied by a mode with $k = 0$. Modes with $k \neq 0$ can only satisfy the homogeneous boundary condition,

$$\psi = 0 \quad \text{at} \quad y = L, \quad 0 < x < x_0. \tag{2.6}$$

The mode with $k = 0$ (the zero or Kelvin mode) has infinite Rossby radius, phase speed and wavelength, this being an artifact of the rigid-lid approximation.

Beyond the shelf/slope region, we impose an approximate outer boundary condition, $u = 0$ at $y = 1$. This boundary condition has been justified in Buchwald and Adams (1968, p. 248) and used in the wind-forced shelf wave studies of Adams and Buchwald (1969) and Gill and Schumann (1974).

We summarize the boundary conditions on Φ in the four regions I, II, III, IV as defined in Fig. 1b.

$$\text{I, IV:} \quad \Phi_n = 0 \quad \text{at} \quad y = 0, \quad \Phi_n' = 0 \quad \text{at} \quad y = 1 \tag{2.7}$$

$$\text{II:} \quad \left.\begin{matrix}\Phi_n = 0\\ \Phi_0 = 0\end{matrix}\right\} \text{ at } y = 0, \quad \left.\begin{matrix}\Phi_n = 0\\ \Phi_0 = B_0\end{matrix}\right\} \text{ at } y = L \tag{2.8}$$

$$\text{III:} \quad \left.\begin{matrix}\Phi_n = 0\\ \Phi_0 = B_0\end{matrix}\right\} \text{ at } y = L, \quad \left.\begin{matrix}\Phi_n' = 0\\ \Phi_0' = 0\end{matrix}\right\} \text{ at } y = 1 \tag{2.9}$$

where $n = 1, 2, 3, \ldots$, and Φ_0 denotes the zero mode.

With $h > 0$, $dh/dy > 0$ and piecewise continuous, Eq. (2.3) plus the homogeneous boundary conditions in (2.7)–(2.9) belong to the class of Sturm-Liouville problems (e.g., see Boyce and Di Prima, 1969). Thus for each of the four regions, the set of functions $\Phi_n(y)$ $(n = 1, 2, \cdots)$ forms a complete orthonormal basis, with

$$\int \frac{h'}{h^2}\Phi_n(y)\Phi_m(y)dy = \delta_{nm} \tag{2.10}$$

where δ_{nm} is the Kronecker delta function.

For the zero mode with $k = 0$, (2.3) reduces to

$$\left(\frac{1}{h}\Phi_0'\right)' = 0, \tag{2.11}$$

which can be integrated twice to yield

$$\Phi_0 = C_1 \int_0^y h dy' + C_2 \tag{2.12}$$

where C_1 and C_2 are constants. From the boundary conditions (2.8) in region II, we obtain[2]

[2] Superscripts I–IV identify the appropriate region.

$$\Phi_0^{II} = B_0 \int_0^y h dy' \Big/ \int_0^L h dy'. \tag{2.13}$$

In region III, (2.9) compels

$$\Phi_0^{III} = B_0, \tag{2.14}$$

which does not support a zero mode as both velocity components are identically zero by (2.2). Similarly, (2.7) eliminates the zero mode in regions I and IV by making $\Phi_0 \equiv 0$. Thus, the zero mode can only be excited in region II.

3. The general solution

In region I, we have an incident shelf wave of mode m,

$$\psi = A\Phi_m^I(y) \exp(ik_m^I x - i\omega t). \tag{3.1}$$

For matching at $x = 0$ and $x = x_0$ (see Fig. 1), we require p and the normal velocity u to be continuous. From (2.1b) and the second equation in (2.2), this amounts to ψ and ψ_y continuous at $x = 0$ and x_0. Because $\Phi(y)$ is continuously differentiable, ψ continuous across $x = 0$ or x_0 automatically implies ψ_y continuous. The alongshore geostrophy approximation assumes v to be small compared to u, so v and ψ_x are allowed to be discontinuous at $x = 0$ and x_0.

In region II,

$$\psi = [\Phi_0^{II}(y) + \sum_{n=1}^{\infty} B_n \Phi_n^{II}(y) \exp(ik_n^{II} x)] e^{-i\omega t}. \tag{3.2}$$

Matching (3.1) and (3.2) across $x = 0$ requires

$$A\Phi_m^I(y) = \Phi_0^{II}(y) + \sum_{n=1}^{\infty} B_n \Phi_n^{II}(y). \tag{3.3}$$

At the barrier $y = L$, (3.3) reduces to

$$A\Phi_m^I(L) = \Phi_0^{II}(L) = B_0, \tag{3.4}$$

which fixes B_0 in terms of the incident wave. The function

$$F(y) \equiv A\Phi_m^I(y) - \Phi_0^{II}(y) \tag{3.5}$$

satisfies the homogeneous boundary condition $F = 0$ at $y = 0$ and L, and can be expressed in terms of the complete orthonormal basis $\{\Phi_n^{II}\}$, i.e.

$$F(y) = \sum_{n=1}^{\infty} B_n \Phi_n^{II}(y),$$

$$B_n = \int_0^L \frac{h'}{h^2} F(y) \Phi_n^{II}(y) dy. \tag{3.6}$$

With B_0 and B_n given by (3.4) and (3.6), the wave field in region II is known.

Similarly, in region III, by (2.14),

$$\psi = [B_0 + \sum_{n=1}^{\infty} C_n \Phi_n^{III}(y) \exp(ik_n^{III} x)] e^{-i\omega t}. \tag{3.7}$$

Matching (3.1) and (3.7) across $x = 0$ yields

$$C_n = \int_L^1 \frac{h'}{h^2} [A\Phi_m^I(y) - B_0] \Phi_n^{III}(y) dy. \tag{3.8}$$

In region IV,

$$\psi = \sum_{n=1}^{\infty} D_n \Phi_n^{IV}(y) \exp[i(k_n^{IV} x - \omega t + \delta_n)], \tag{3.9}$$

matching of (3.2) and (3.7) with (3.9) across $x = x_0$ yields

$$D_n \exp[i(k_n^{IV} x_0 + \delta_n)] = \int_0^L \frac{h'}{h^2} [\Phi_0^{II} + \sum_{j=1}^{\infty} B_j \Phi_j^{II} \exp(ik_j^{II} x_0)] \Phi_n^{IV} dy + \int_L^1 \frac{h'}{h^2} [B_0 + \sum_{j=1}^{\infty} C_j \Phi_j^{III} \exp(ik_j^{III} x_0)] \Phi_n^{IV} dy. \tag{3.10}$$

For a general monotonically increasing depth profile $h(y)$ and a given frequency ω, the corresponding wavenumbers $\{k_n\}$ and the eigenfunctions $\{\Phi_n\}$ in each region can be obtained numerically, (Caldwell and Longuet-Higgins, (1971)). The Φ_0^{II} is computed from (2.13), and the problem is solved as we know B_0, B_n, C_n and D_n from (3.4), (3.6), (3.8) and (3.10).

Energy flux and orthogonality relations are discussed in Huthnance (1975, Section 5) under three distinct cases—(i) ω specified, (ii) k specified and (iii) c specified. For our wave scattering problem, ω is fixed, hence Huthnance's case (i) results apply. He proved that the energy flux separates into contributions from individual modes, but that the energy density E does not necessarily separate into individual modal contributions, i.e. there may be interaction energies between modes. We have however used more restrictive equations than Huthnance. The alongshore geostrophy approximation (2.1b) which amounts to taking the nondispersive long wave limit, and the rigid lid approximation reduce the (alongshore averaged) energy density E to

$$E = \int hu^2 dy, \tag{3.11}$$

i.e. onshore current and surface elevation contribute negligible energy. Then Huthnance [1975, p. 699, case (i)] shows that E also separates into individual modal contributions since

$$\int hu_m u_n dy = 0 \tag{3.12}$$

for $m \neq n$.

Substitute (2.2) for u in (3.11), average alongshore, then integrate (3.11) by parts, and upon invoking (2.3), (2.11) and (2.10), obtain the energy density

$$E^{II} = \frac{1}{2}\left[B_0^2\left(\int_0^L hdy\right)^{-1} + \sum_{n=1}^{\infty} B_n^2/c_n^{II}\right],$$

$$E^{III} = \frac{1}{2}\sum_{n=1}^{\infty} C_n^2/c_n^{III},$$

$$E^{IV} = \frac{1}{2}\sum_{n=1}^{\infty} D_n^2/c_n^{IV}, \tag{3.13}$$

where c_n is the nth mode phase speed in the appropriate region.

4. On exponential topography

We now examine a specific case, where the bottom topography increases exponentially offshore,

$$h = h_0 e^{2by}, \quad 0 \leq y \leq 1, \tag{4.1}$$

as studied by Buchwald and Adams (1968). Equation (2.3) becomes

$$\Phi'' - 2b\Phi' + \frac{2b}{c}\Phi = 0. \tag{4.2}$$

Assuming $\Phi \propto e^{\lambda y}$, λ satisfies

$$\lambda = b \pm i\gamma, \quad \gamma = (2b/c - b^2)^{1/2}, \tag{4.3}$$

whence

$$c = 2b/(\gamma^2 + b^2), \quad k = \omega(\gamma^2 + b^2)/(2b). \tag{4.4}$$

In regions I and IV, the boundary conditions (2.7) give

$$\Phi_n^{I} = A_n^{I} e^{by} \sin\gamma_n^{I} y, \quad n = 1, 2, \cdots, \tag{4.5}$$

with γ_n^{I} satisfying

$$\tan\gamma_n = -\gamma_n/b. \tag{4.6}$$

Figure 2 gives the values for γ_n over a reasonable range of b values. The orthonormal relation (2.10) over the range $0 \leq y \leq 1$ yields the normalization factor

$$A_n^{I} = \left[\frac{2h_0\gamma_n}{b(2\gamma_n - \sin 2\gamma_n)}\right]^{1/2}. \tag{4.7}$$

Similarly, in region III, boundary conditions (2.9) yield

$$\Phi_n^{III} = A_n^{III} e^{by} \sin\gamma_n^{III}(y - L) \tag{4.8}$$

with γ_n^{III} satisfying

$$\tan\gamma_n(1 - L) = -\frac{\gamma_n(1 - L)}{b(1 - L)}. \tag{4.9}$$

Since (4.9) is identical to (4.6) upon defining $\tilde{\gamma}_n = \gamma_n(1 - L)$ and $\tilde{b} = b(1 - L)$, values of γ_n^{III} can thus be obtained from Fig. 2. Orthonormality over the range $L \leq y \leq 1$ gives

$$A_n^{III} = \left\{\frac{2h_0\gamma_n}{b[2\gamma_n(1 - L) - \sin 2\gamma_n(1 - L)]}\right\}^{1/2}. \tag{4.10}$$

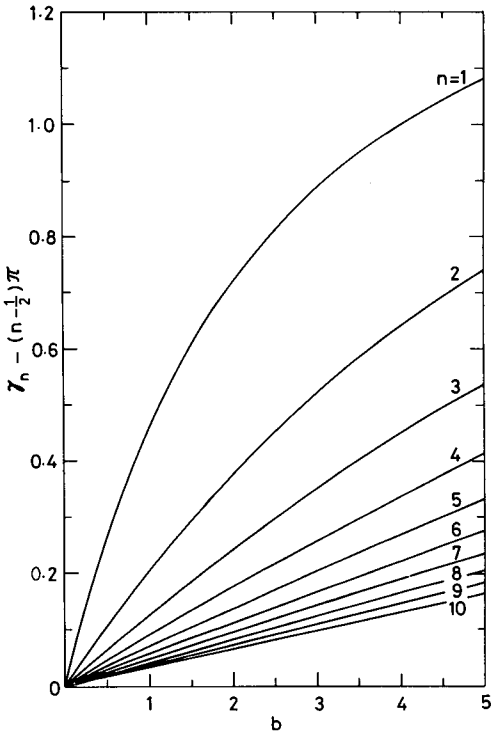

FIG. 2. Values of γ_n as a function of the exponential topography parameter b, for $n = 1, \ldots, 10$. The actual values plotted on the y-axis are $\gamma_n - [n - (1/2)]\pi$. With this diagram, the solution in Section 4 can be readily applied to continental shelves of different b values.

In region II, (2.8) yields

$$\Phi_n^{II} = A_n^{II} e^{by} \sin n\pi y/L,$$

$$A_n^{II} = \left(\frac{h_0}{bL}\right)^{1/2}, \quad n = 1, 2, \cdots. \tag{4.11}$$

For mode 0, (2.13) gives

$$\Phi_0 = B_0 \frac{e^{by}\sinh by}{e^{bL}\sinh bL}. \tag{4.12}$$

Upon integrating (3.6) and (3.8), we obtain the scattering coefficients B_n and C_n,

$$B_n = \frac{2bL}{h_0} AA_m^{I} A_n^{II} \sin(\gamma_m L)(-1)^n n\pi \times \left[\frac{1}{(\gamma_m L)^2 - (n\pi)^2} + \frac{1}{(bL)^2 + (n\pi)^2}\right], \tag{4.13}$$

$$C_n = \frac{2b}{h_0} AA_m^{I} A_n^{III}\left\{\frac{1}{2}\left[\frac{\sin[\gamma_m - \gamma_n(1 - L)]}{\gamma_m - \gamma_n} - \frac{\sin[\gamma_m + \gamma_n(1 - L)]}{\gamma_m + \gamma_n} - \frac{2\gamma_n \sin\gamma_m L}{\gamma_m^2 - \gamma_n^2}\right] - \frac{\gamma_n \sin\gamma_m L}{b^2 + \gamma_n^2}\right\}, \tag{4.14}$$

where for abbreviation, $\gamma_m = \gamma_m^{\mathrm{I}}$, and $\gamma_n = \gamma_n^{\mathrm{III}}$, $n = 1, 2, \ldots$. From (3.4),

$$B_0 = AA_m^{\mathrm{I}} e^{bL} \sin(\gamma_m^{\mathrm{I}} L). \tag{4.15}$$

Similarly, upon integrating (3.10), we have

$$D_n \exp[i(k_n^{\mathrm{IV}} x_0 + \delta_n)] = P_n + \sum_{j=1}^{\infty} B_j \exp(ik_j^{\mathrm{II}} x_0) Q_{nj} + \sum_{j=1}^{\infty} C_j \exp(ik_j^{\mathrm{III}} x_0) R_{nj}, \tag{4.16}$$

where (since $\Phi^{\mathrm{I}} = \Phi^{\mathrm{IV}}$, $\gamma^{\mathrm{I}} = \gamma^{\mathrm{IV}}$),

$$P_n = \int_0^L \frac{h'}{h^2} \Phi_n^{\mathrm{I}} \Phi_0^{\mathrm{II}} dy + \int_L^1 \frac{h'}{h^2} \Phi_n^{\mathrm{I}} \Phi_0^{\mathrm{III}} dy = \frac{2b^2}{h_0} AA_n^{\mathrm{I}} A_m^{\mathrm{I}} \frac{\sin\gamma_m L}{b^2 + \gamma_n^2} \sin\gamma_n L(\coth bL + 1),$$

$$Q_{nj} = \int_0^L \frac{h'}{h^2} \Phi_n^{\mathrm{I}} \Phi_j^{\mathrm{II}} dy = \frac{2bL}{h_0} A_n^{\mathrm{I}} A_j^{\mathrm{II}} \sin\gamma_n L(-1)^j \frac{j\pi}{(\gamma_n L)^2 - (j\pi)^2},$$

$$R_{nj} = \int_L^1 \frac{h'}{h^2} \Phi_n^{\mathrm{I}} \Phi_j^{\mathrm{III}} dy = \frac{b}{h_0} A_n^{\mathrm{I}} A_j^{\mathrm{III}} \left\{ \frac{\sin[\gamma_n - \gamma_j(1-L)]}{\gamma_n - \gamma_j} - \frac{\sin[\gamma_n + \gamma_j(1-L)]}{\gamma_n + \gamma_j} - \frac{2\gamma_j \sin\gamma_n L}{\gamma_n^2 - \gamma_j^2} \right\},$$

with $\gamma_m = \gamma_m^{\mathrm{I}}$, $\gamma_n = \gamma_n^{\mathrm{I}}$, and $\gamma_j = \gamma_j^{\mathrm{III}}$, $n = 1, 2, \ldots$.

From (3.13), the energy density of mode n normalized with respect to the incident energy is given by

$$E_0^{\mathrm{II}} = bB_0^2(e^{2bL} - 1)^{-1}/E_I(0 < y < L), \tag{4.17a}$$

$$E_n^{\mathrm{II}} = \frac{1}{2} \frac{B_n^2}{c_n^{\mathrm{II}}} \Big/ E_I(0 < y < L), \tag{4.17b}$$

$$E_n^{\mathrm{III}} = \frac{1}{2} \frac{C_n^2}{c_n^{\mathrm{III}}} \Big/ E_I(L < y < 1), \tag{4.17c}$$

$$E_n^{\mathrm{IV}} = \frac{1}{2} \frac{D_n^2}{c_n^{\mathrm{IV}}} \Big/ E_I(0 < y < 1), \tag{4.17d}$$

where c_n is given by (4.4) in each region, and the incident energy density into the cross section $a_1 < y < a_2$ is given by

$$E_I(a_1 < y < a_2) = \int_{a_1}^{a_2} hu^2 dy. \tag{4.18}$$

In particular,

$$E_I(0 < y < L) = \frac{1}{2h_0} AA_m^2 \left[\frac{L}{2}(b^2 + \gamma_m^2) + \frac{\sin 2\gamma_m L}{4\gamma_m}(-b^2 + \gamma_m^2) + b \sin^2\gamma_m L \right], \tag{4.19}$$

where $A_m = A_m^{\mathrm{I}}$ and $\gamma_m = \gamma_m^{\mathrm{I}}$. $E_I(0 < y < 1)$ is obtained from (4.19) by setting $L = 1$, and $E_I(L < y < 1) = E_I(0 < y < 1) - E_I(0 < y < L)$. This normalization ensures

$$E_0^{\mathrm{II}} + \sum_{n=1}^{\infty} E_n^{\mathrm{II}} = 1, \quad \sum_{n=1}^{\infty} E_n^{\mathrm{III}} = 1, \quad \text{and} \quad \sum_{n=1}^{\infty} E_n^{\mathrm{IV}} = 1. \tag{4.20}$$

Next, we illustrate some features of our solution. Choose a typical value $b = 2$, (e.g. for the relatively steep shelf off Sydney, Buchwald and Adams, 1968, obtained $b = 2.7$, whereas off Oregon, Hsieh and Mysak, 1980, obtained $b = 1.65$). For an incident shelf wave of mode $m = 1$, Fig. 3 illustrates how changing the offshore location L of the barrier affects the energy distribution in region II. Except for relatively large L, (barrier far from the coast), the incident first mode energy is essentially all transferred to the zeroth mode, in agreement with the step-shelf model of HB. In region III, the incident energy remains

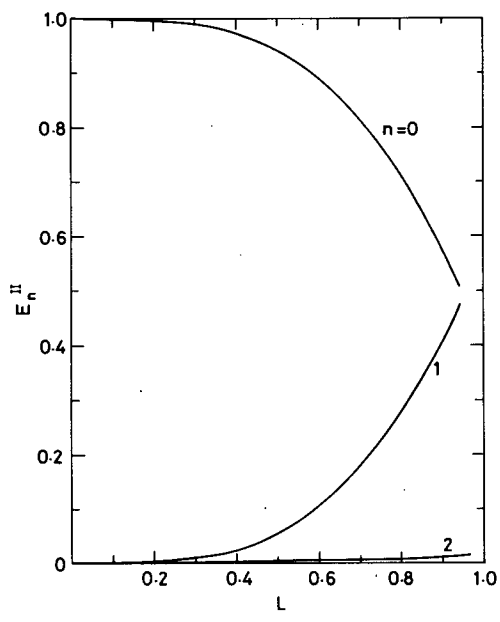

FIG. 3. E_n^{II}, the normalized mode n energy density in region II for $n = 0$, 1 and 2, plotted as a function of L, the offshore location of the barrier. The incident first mode ($m = 1$) shelf wave transfers its energy readily to the $n = 0$ mode in region II.

essentially in mode 1 while changing L, with $E_1^{III} > 0.97$ for $0 \leqslant L < 1$.

The scattering behaviour is easily understood when we examine the offshore modal structures, shown in Fig. 4 for the barrier located at $L = 0.3$. Since we require ψ continuous across $x = 0$, it is clear from Fig. 4 that the $n = 0$ mode in region II and the $n = 1$ mode in region III match most readily with the $m = 1$ incident mode because of their physical resemblance to the incident mode. Hence, the incident energy is scattered mainly into the $n = 0$ mode in II and the $n = 1$ mode in III.

Figure 5 shows the energy distribution in region II when the incident wave is of mode $m = 2$. For L small (barrier close to coast), the dominant mode excited is still the $n = 0$ mode. Only when L is relatively large before the $n = 1$ mode becomes dominant. In region III, Fig. 6 shows that for L small, the incident energy stays in the second mode as expected, but for larger L, much of the second mode incident energy is transferred to then $n = 1$ mode. Hence an alongshore barrier can be very effective in transferring incident energy to other modes.

What happens downstream from the barrier, i.e. in region IV? The behaviour now depends not only on L, but also on the length x_0 of the barrier relative to the incident wavelength. By (4.4), all waves in our system are nondispersive, so the entire alongshore picture scales linearly with ω^{-1}. Hence, the parameter ωx_0 indicates the relative length of the barrier. With an incident $m = 1$ wave, the first-mode energy in region IV is plotted as a function of L in Fig. 7 for $\omega x_0 = 0.1$, 0.3 and 1. For a relatively short barrier, $\omega x_0 = 0.1$, most of the incident first mode energy

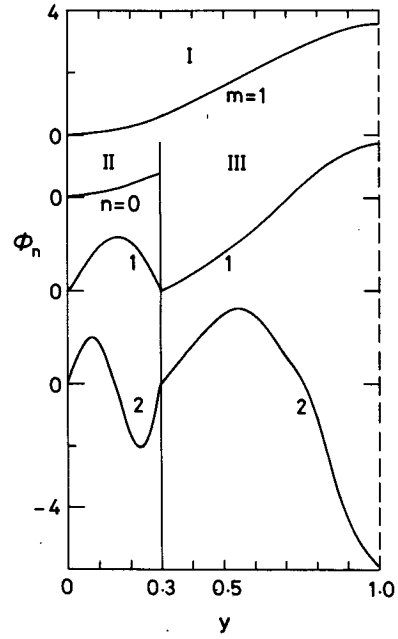

FIG. 4. Offshore structures of Φ_n. The $m = 1$ incident mode in region I is shown on top. Below are shown the first few modes in regions II and III, with the barrier located at $L = 0.3$. It is clear that the $n = 0$ mode in region II and the $n = 1$ mode in III match most readily with the $m = 1$ incident mode from I.

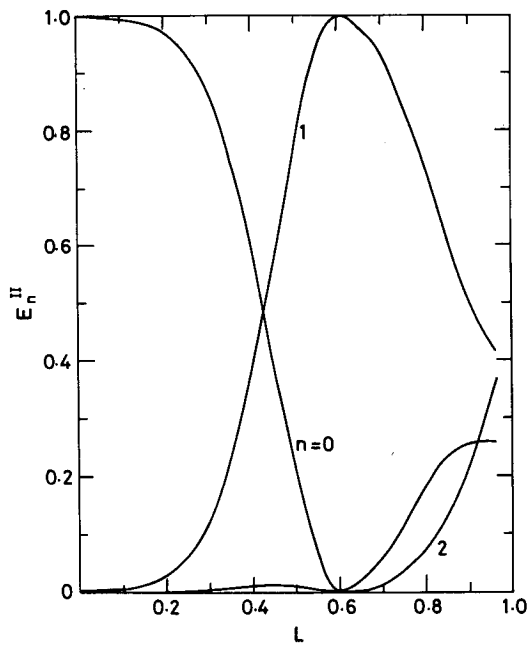

FIG. 5. E_n^{II} as a function of L, with an incident wave of mode $m = 2$. The $n = 0$ mode remains dominant in region II for L small, but yields to the $n = 1$ mode for larger L.

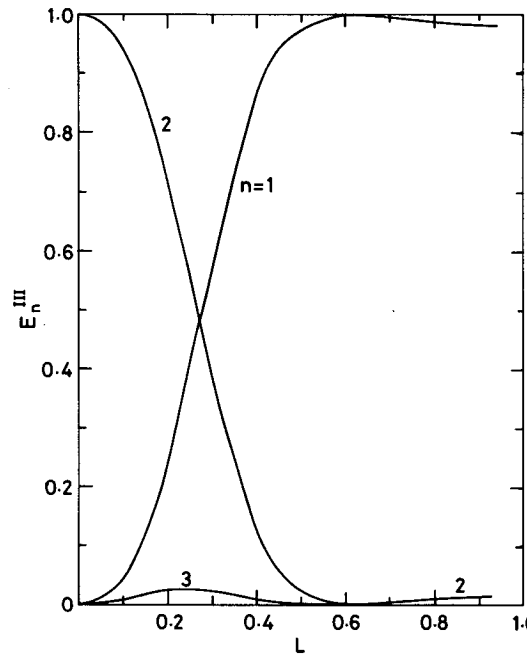

FIG. 6. E_n^{III} as a function of L, with an incident $m = 2$ wave. For relatively large L, the incident second mode energy is mainly converted to first mode energy in region III.

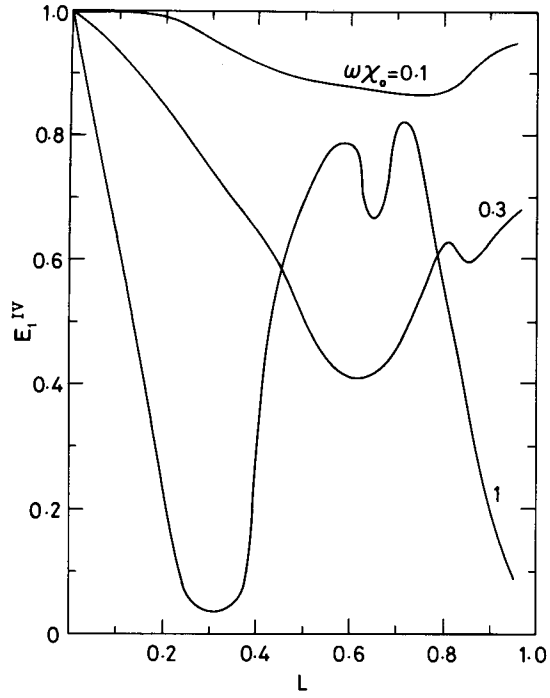

FIG. 7. E_1^{IV}, the $n = 1$ mode energy in region IV, as a function of L for 3 values of ωx_0, the relative length of the barrier. The incident wave is of mode $m = 1$. As ωx_0 increases from 0.1 to 0.3, the curve drops, indicating more energy is scattered out of the first mode as the barrier becomes longer. The curve becomes progressively more oscillatory as ωx_0 increases.

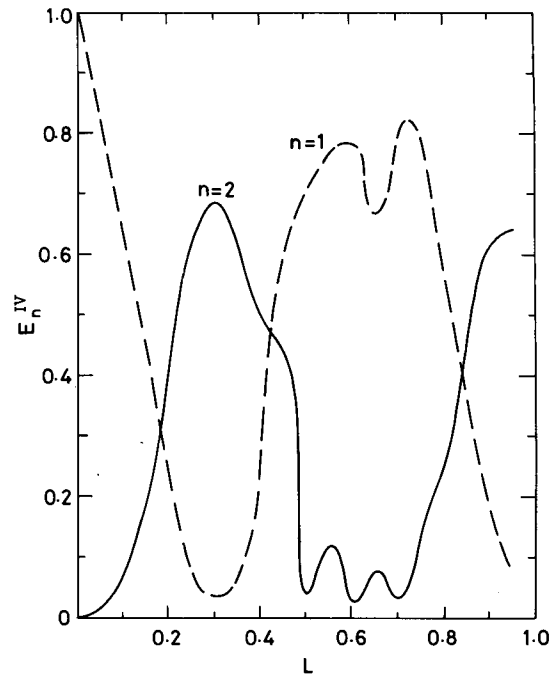

FIG. 8. E_n^{IV} for $n = 1$ and 2 with $\omega x_0 = 1$, ($m = 1$). A sharp minimum of the $n = 1$ mode (dashed curve) develops at $L \approx 0.3$, where nearly 70% of the energy is in the $n = 2$ mode (solid curve).

remains in the first mode after passing the barrier. As ωx_0 increases, the E_1^{IV} curve develops progressively more and more extrema. For $\omega x_0 = 1$, at $L \approx 0.3$, a minimum in E_1^{IV} is manifest, and the energy is now mainly transferred to the second mode, as illustrated in Fig. 8. Thus, for a long enough barrier, much of the incident energy may be permanently transferred to a different mode after passing the barrier. Furthermore, the incident wave may undergo substantial phase shift upon passing the barrier, as illustrated in Fig. 9.

5. Approximations and limitations of the theory

The full scattering problem at subinertial frequencies is extremely complex because three types of waves with very different length scales are involved—evanescent Poincaré waves at small scales, long and short shelf waves at intermediate scales, and Kelvin waves at large scales. The rigid lid eliminates the Poincaré waves and the Kelvin waves (except that in region II which becomes the zeroth mode), while the alongshore geostrophy assumption removes the short shelf waves.

At subinertial frequencies, the Poincaré waves generated at the tip of the barrier decay with distance. In a flat-bottom channel of width L, a Poincaré wave of mode n with $\omega < f$ decays along channel with a e-folding distance

$$l = \left(\frac{f^2 - \omega^2}{gH} + \frac{n^2\pi^2}{L^2}\right)^{-1/2} \tag{5.1}$$

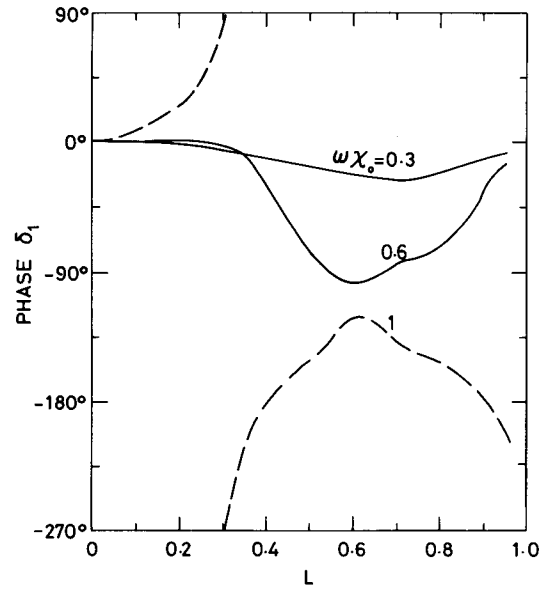

FIG. 9. The anomalous phase shift δ_1 [defined in (3.10)] for the first mode upon passing the barrier, plotted as a function of L for $\omega x_0 = 0.3$, 0.6 and 1. For $\omega x_0 = 1$, the minimum at $L \approx 0.3$ produces a rapid phase change.

derived from LeBlond and Mysak [1978, Eq. (28.8)]. For $H \sim 10^2$–10^3 m, $f \approx 10^{-4}$ s^{-1}, $L \leqslant 100$ km,

$$l \approx \frac{L}{n\pi}. \tag{5.2}$$

For $n = 1$, $l \approx 10$ km for $L = 30$ km, i.e. for the barrier located at 30 km offshore, the influence of the Poincaré waves generated at the tip extends only about 10 km into region II. Having omitted the evanescent Poincaré waves, our model would be inaccurate near the tip of the barrier.

For a chain of islands running parallel to the coast, our eigenfunction matching technique can be repeated for each island, provided the islands and the distances separating them are long compared to the Poincaré wave e-folding distance. As a model for the Great Barrier Reef, our theory is not entirely satisfactory since the Great Barrier Reef is not an impenetrable barrier (see Middleton, 1983), and its myriad of small coral reefs ensures a continuous generation of evanescent Poincaré waves.

The Kelvin wave in regions I, III and IV has been eliminated by the rigid lid and the outer boundary condition ($u = 0$ at $y = 1$). In reality, we would not expect significant energy transfer between the shelf waves and the Kelvin wave in these regions because of the drastic difference in the offshore extent of the Kelvin wave and the shelf waves. In region II, where the energy transfer can be substantial, the Kelvin wave is restricted by the rigid lid to have $k = 0$ (infinite wavelength). However, with respect to the shelf-wave scales, the Kelvin wave does not have very long wavelength, i.e. $k \approx 0$. So a $k = 0$ model is crude, but not unreasonable.

The alongshore geostrophy approximation (2.1b), which renders all shelf wave modes nondispersive, is poor at short wavelength. In particular, the short shelf waves with negative group velocities are absent in our model. These short waves represent backscatter of the incident wave energy, and their absence leads to inaccurate energy transmission. For instance, in the case $\omega x_0 = 1$, $L \approx 0.3$ shown in Fig. 8, the energy in region IV is mainly in the second mode with energy density $E_2^{IV} \approx E_I$, the incident first mode energy density. But the energy flux $c_{g2}E_2^{IV}$ is much less than the incident flux $c_{g1}E_I$ because c_{g2}, the group velocity of the second mode, is much less than c_{g1}. The missing energy flux is presumably reflected back by the short waves, which are not represented in our model.

6. Summary

From the unforced, inviscid barotropic shallow water equations under rigid-lid and alongshore geostrophy approximations, the scattering of an incident continental shelf wave by a long thin offshore barrier lying parallel to the coastline has been solved for any general topography $h(y)$ satisfying $h > 0$, $h' > 0$ and piecewise continuous. In particular, simple analytic formulas for the scattering coefficients are derived for the exponential shelf.

The most intriguing prediction of our theory is that in region II, between the barrier and the coast, much of the incident shelf wave energy would be converted to the $n = 0$ Kelvin mode, (in agreement with the earlier model of HB). Physically, the condition of zero onshore flow ($v = 0$) at the barrier and at the coast renders the excitation of modes with substantial v in the channel (region II) difficult, especially when the channel is narrow. The Kelvin mode with relatively negligible v compared to the shelf wave modes is thus favourably excited in region II. Recent observations off New South Wales during the Australian Coastal Experiment (ACE) suggest that much subinertial energy emerges from Bass Strait. Our theory suggests that incident shelf waves from South Australia would be scattered into the Kelvin mode within Bass Strait before reemerging downstream as shelf waves off New South Wales.

Even though the Kelvin wave is not properly modeled here because of the rigid-lid approximation, the transfer of energy from the incident shelf wave to the Kelvin wave in region II is likely to be real and testable observationally. The Kelvin wave, a rotationally trapped gravity wave, can be readily distinguished from the shelf waves by its relatively large ratio of sea level displacement to current amplitude (Hsieh, 1985, Appendix). Hence, if anomalously large ratios of sea level to current fluctuations of subinertial frequencies are observed in region II but not in regions I or IV, our prediction would be confirmed.

In region III, seaward of the barrier, substantial energy transfer from an incident second-mode wave to the first mode is also possible. When the barrier length is short relative to the incident wavelength, the incident wave suffers only small energy loss and a slight phase shift upon emerging from the downstream end of the barrier. When the barrier length is increased, the incident mode may vanish downstream, leaving a different mode to dominate in region IV.

Acknowledgment. One of us (WWH) is grateful to the Australian Queen's Fellowship and Marine Research Allocation Advisory Committee for its support by the award of a Queen's Fellowship in Marine Science.

REFERENCES

Adams, J. K., and V. T. Buchwald, 1969: The generation of continental shelf waves. *J. Fluid Mech.* **35,** 815–826.

Allen, J. S., 1976: Continental shelf waves and alongshore variations in bottom topography and coastline. *J. Phys. Oceanogr.*, **6,** 864–878.

Boyce, W. E., and R. C. DiPrima, 1969: *Elementary Differential Equations and Boundary Value Problems.* 2nd ed., Wiley, 533 pp.

Brink, K. H., 1980: Propagation of barotropic continental shelf waves over irregular bottom topography. *J. Phys. Oceanogr.*, **10,** 765–778.

Buchwald, V. T., 1977: Diffraction of shelf waves by an irregular coastline. *Lecture Notes in Physics,* D. G. Provis and R. Radok, Eds., Springer, **64,** 188–193.

——, and J. K. Adams, 1968: The propagation of continental shelf waves. *Proc. Roy. Soc. London,* **A305,** 235–250.

Caldwell, D. R., and M. S. Longuet-Higgins, 1971: The experimental generation of double Kelvin waves. *Proc. Roy. Soc. London,* **A326,** 39–52.

Chao, S.-Y., L. J. Pietrafesa and G. S. Janowitz, 1979: The scattering of continental shelf waves by an isolated topographic irregularity. *J. Phys. Oceanogr.*, **9,** 687–695.

Davis, A. M. J., 1981: The scattering by a headland of the dominant continental shelf wave. *Phil. Trans. Roy. Soc. London,* **A303,** 383–431.

Gill, A. E., and E. H. Schumann, 1974: The generation of long shelf waves by the wind. *J. Phys. Oceanogr.*, **4,** 83–90.

Grimshaw, R., 1977: The effects of a variable Coriolis parameter, coastline curvature and variable bottom topography on continental shelf waves. *J. Phys. Oceanogr.*, **7,** 547–554.

Hsieh, W. W., 1985: Modal bias in sea level and sea surface temperature, with applications to remote sensing. *J. Phys. Oceanogr.*, **15,** 351–356.

——, and L. A. Mysak, 1980: Resonant interactions between shelf waves, with applications to the Oregon shelf. *J. Phys. Oceanogr.*, **10,** 1729–1741.

——, and V. T. Buchwald, 1984: The scattering of a continental shelf wave by a semi-infinite barrier located along the outer-edge of a step shelf. *Geophys. Astrophys. Fluid Dyn.*, **28,** 257–276.

Huthnance, J. M., 1975: On trapped waves over a continental shelf. *J. Fluid Mech.*, **69,** 689–704.

LeBlond, P. H., and L. A. Mysak, 1978: *Waves in the Ocean.* Elsevier, 602 pp.

Middleton, J. H., 1983: Low-frequency trapped waves on a wide, reef-fringed continental shelf. *J. Phys. Oceanogr.*, **13,** 1371–1382.

Wang, D.-P., 1980: Diffraction of continental shelf waves by irregular alongshore geometry. *J. Phys. Oceanogr.*, **10,** 1187–1199.